Coefficient-Preservation Analysis of Offset Double-Serpentine Exhaust Nozzles

Jawad Javed[1,*] and Maria Jawad[1]

[1] IU International University of Applied Sciences
* Correspondence: b.jawad4891@gmail.com

Abstract: However, offset double-serpentine exhaust nozzles can manipulate the exhaust flow path within restricted propulsion systems, while the aerodynamic quality of such designs cannot be assessed by any coefficient alone. The key issue is the identification of the particular member of the 27-run, four-factor, three-level nozzle design array that maintains the pressure recovery coefficient, discharge coefficient, and axial thrust coefficient at once, and what particular geometric distributions form the limit for the maintenance of the trio of the coefficients. First, the three coefficients of the array will be converted into non-dimensional retention levels of these coefficients with respect to the range between the minimum and maximum levels of the coefficients recorded within L27 table. Next, coefficient preservation index (CPI), lower-tail retention value, response-spread penalty, factor-level contrast, and leave-one-response rank mobility are computed for each configuration. The output is very selective – only configurations 3, 5, and 9 fulfill the conditions CPI $\geq$ 0.90 and lower-tail retention $\geq$ 0.85. Configuration 3 is the single nozzle with complete retention of all the three coefficients, while configurations 5 and 9 provide high triad retention with minimal coefficient imbalance. The factor-level contrasts identify DCV2 and DCS as the controlling factors with the mean CPI level of 0.420 and 0.353 correspondingly. The first vertical distribution (DCV1) is very flat, thus confirming the less significant role of the upstream vertical redistribution against the downstream turning placement.

Keywords: double-serpentine nozzle; exhaust integration; coefficient preservation; L27 orthogonal array; pressure recovery; discharge coefficient; axial thrust coefficient

Citation: Jawad Javed and Maria Jawad. 2023. Coefficient-Preservation Analysis of Offset Double-Serpentine Exhaust Nozzles. *TK Techforum Journal (ThyssenKrupp Techforum)* 2023(3): 35–52.

Received: September-03-2023
Accepted: December-02-2023
Published: December-30-2023

1. Introduction

Exhaust systems for compact propulsion configurations may need to curve, deflect, or otherwise modify the flow before it reaches the exit plane. Curvature, deflection, and offset cause cross-stream pressure gradient, secondary motion, boundary-layer skewing, and separation tendencies that impair pressure recovery and thrust performance [1]. Such losses are caused by the physics of turbulent flow through curved ducts that causes centrifugal imbalance and redistributes stagnation pressure [2]. Early studies of S-shaped ducts revealed that curvature-related secondary flows can persist after the bend and distort the pressure recovery and swirl patterns, particularly for ducts containing more complex curvature sequences rather than a single curved turn [3,4]. These phenomena remain applicable for double-serpentine exhaust ducts since the flow arriving into the last extension already had a complex history of curvature, diffusion, wall shear, and three-dimensional redistribution [5]

Design challenges arise not only from the ability of a serpentine nozzle to lose pressure recovery. In fact, the more difficult problem is that several aerodynamic quantities change in different directions when the same passage is changed. Compressible nozzle theory describes the nozzle operating by means of mass conservation, momentum balance, and stagnation-to-static change [6], but the actual exhaust components are rarely one-dimensional devices. Wall curvature, finite boundary-layer, local diffusion, and turning cause the exit state to depend on the passage through which the flow passes. A geometry

that gives high discharge coefficient and low thrust is not necessarily good, as a geometry that produces high thrust but low pressure recovery. Hence, it is important for compact nozzles and serpentine ducts to consider pressure recovery, discharge coefficient, and thrust simultaneously [7].

Offset double-serpentine nozzles are especially sensitive to this coupled consideration since the useful geometric features of this nozzle type also introduce corresponding aerodynamic penalties. The double offset allows integrating the exhaust system in a compact propulsion layout, but the double offset causes the passage curvature and turning memory effect, and non-uniformity of the flow approaching the final contraction. In an axisymmetric nozzle, the designer may think about area ratio, contraction smoothness, and choking effects. In the current family of geometries, however, the area distribution, first vertical redistribution, second vertical redistribution, and spanwise redistribution take place at different stations along an already distorted passage. Downstream design controls operate not on an unperturbed incoming field; they operate on a perturbed field caused by the upstream curvature. Therefore, the most appropriate design cannot be identified by the level of only one geometric factor or the largest single coefficient.

Duct aerodynamics literature confirms this multi-location interpretation. Numerous studies of S-ducts revealed that pressure loss and flow distortion depend not only on the total bend angle but on the sequence of curvature, diffusion, and wall pressure recovery along the passage [8]. Further, turbulent secondary-flow theory revealed that the most substantial penalty occurs when a downstream geometric feature intensifies, rather than weakens an already developed cross-flow pattern. For double-serpentine nozzles, it means that the second vertical redistribution and the spanwise redistribution have more leverage over the final triad of coefficients than an upstream feature having the same nominal level. Therefore, the design matrix has to be interpreted with respect to the location of each factor level along the passage.

Second, there is the question about how to interpret the design matrix. Orthogonal experimental designs provide efficient factor level distributions and first-order response surface analysis without the need for complete factorial experiment [9]. The response surface methodology and robust-design literature suggests that such designs should be analyzed not only by the best run but also by factor contrasts, response dispersion, and objective function sensitivity [10]. For an offset double-serpentine nozzle, it means that the best-looking case must be checked whether it is good enough by considering the pressure recovery, discharge coefficient, and axial thrust coefficient. Rank obtained from a single coefficient can have some meaning in nozzle selection, but it is incomplete if the candidate has to perform several aerodynamic functions.

Several methods of multi-response decision making can combine competing objectives using desirability functions, value-based decision models, multi-criteria analysis, and physical programming [11,12]. These techniques share a common point - a single response score is helpful only when the analyst understands how it was obtained. A candidate can be uniformly good or compensate for a weakness of one coefficient by advantages of two others. In nozzle selection, compensation is risky since the weakest coefficient retained in the selection can become the limiting aerodynamic characteristic in future design. Moreover, sensitivity analysis and model validation literature emphasizes that rank persistence should be checked before drawing design rules from a finite numerical table [13,14]. Therefore, the three coefficients are considered here as a preservation triad rather than as separate objectives [15].

Preservation of coefficients vs. coefficient maximization is an essential aspect of the article. In ordinary single-response selection, the analyst can pick up the case with the largest C_d or C_f and analyze the remaining coefficients later. This approach is not sufficient for the offset exhaust system since a downstream design choice can increase one coefficient at the cost of weakening another by affecting the same flow structures. The current interpretation considers the three coefficients as a single aerodynamic signature. A candidate is strong only when the signature is high in all three coordinates. That is why

lower-tail value is used in addition to CPI since it can prevent the analysis from praising a candidate with only an averaged strong signature.

The term preservation is used in a strict numerical sense. It neither implies a comparison with some external geometry, nor requires a calculation of some ideal flow. It means that each geometry is evaluated according to its capability to retain each coefficient relatively to the best and weakest values obtained among all members of the same L27 family. This internal normalization is advantageous for a compact comparative study since it keeps the conclusion limited to the actually explored design space. It also avoids the possible ambiguity of placing pressure recovery, discharge coefficient, and thrust coefficient on different scales.

The article considers a specific design question: *which coded offset double-serpentine nozzle configurations preserve pressure recovery, discharge coefficient, and axial thrust coefficient simultaneously, and which distribution factors define the high-preservation region of the design array?* The answer is derived from the complete L27 coefficient table for a four-factor, three-level nozzle family. The analysis converts each coefficient into a nondimensional retention value, calculates the coefficient preservation index (CPI), preserves the weakest retained coefficient with the help of lower-tail test, evaluates the response imbalance, analyzes factor-level means, and checks rank persistence with the removal of one coefficient at a time. The objective is not to select the best response, but to reveal those nozzle configurations having a strong aerodynamic signature provided by the whole coefficient triad.

The article also avoids treatment of the 27 cases as a black box. Each numerical output is explained by the coded geometry. If a candidate performs well, its A, B, C, and D factors are checked to find the repeating pattern of success. If a candidate performs poorly, the retention values are used to detect if the poor performance is caused by a poor retention of only one aerodynamic coefficient. This approach keeps the manuscript oriented to the actual nozzle family, not to some abstract optimization goal.

Such orientation gives the article two practical roles. First, it gives a compact way to select L27 members for flow-field analysis. Second, it gives the factor-level explanation of the selection and not just an isolated ranking. The interpretation of the results separates the candidates with a uniform aerodynamic quality from those candidates that look good only partially. Since all calculations are based on the actual coefficient values of the 27 configurations, the design statement is numerical: the preferred set of geometries is defined by its simultaneous retention of pressure recovery, discharge coefficient, and axial thrust coefficient.

2. Matrix of nozzles and the development of responses

2.1. Geometrical coding

The studied nozzle family includes an entry part, two redistributions on vertical centerlines, a spanwise redistribution, and a part after the spanwise redistribution. Four coded variables are introduced as follows: area distribution (DA), vertical centerline distribution number 1 (DCV1), vertical centerline distribution number 2 (DCV2), and spanwise centerline distribution (DCS). There are three levels for each variable, which results in the L27 arrangement presented in Appendix A and placed geometrically in Figure 1.

Table 1. Factor coding.

Code	Factor	Level 1	Level 2	Level 3
A	DA, area distribution	Exit-concentrated change	Moderated change	Entrance-concentrated change
B	DCV1, first vertical distribution	Exit-concentrated change	Moderated change	Entrance-concentrated change
C	DCV2, second vertical distribution	Exit-concentrated change	Moderated change	Entrance-concentrated change
D	DCS, spanwise distribution	Exit-concentrated change	Moderated change	Entrance-concentrated change

In contrast, the coding scheme used in Table 1 is symmetric between the four factors, while the physical interpretation is not necessarily so. All three levels have identical descriptions in terms of descriptive significance, but their aerodynamic effects will differ de-

pending upon where in the streamwise direction they appear. DA controls the distribution of the change in passage area. DCV1 affects the flow during its early vertical redistribution, when it has not been fully subject to the double-serpentine configuration. DCV2 follows the first redistribution and thus acts on a more mature non-uniform flow state. DCS affects spanwise redistribution in the region near where the downstream extension receives the flow. This difference is crucial because the effect of the same factor level can be quite different depending on whether it appears upstream or downstream.

The factor description makes clear why the L27 configuration is an appropriate starting point for the current coefficient preservation analysis. There are 81 designs within the full factorial design with four factors and three levels per factor. The L27 form provides sufficient compactness without excluding the ability to have every level of every factor repeated and balanced. Such balance is necessary for factor level means. If a level of a factor occurs in combination with a rare level of another factor, the CPI for that factor level should not be overly dominated by such combinations. While the orthogonal arrangement cannot answer all questions about interactions, it does ensure a structured numeric way to compare trends at the levels of DA, DCV1, DCV2, and DCS.

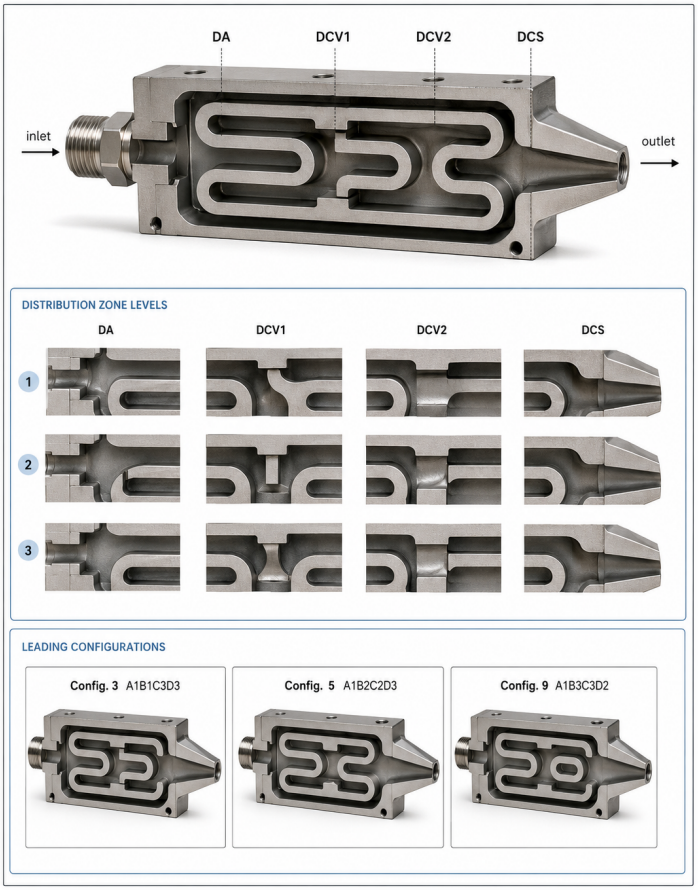

Figure 1. Coded nozzle architecture.

In the architectural representation of Figure 1, the four codes are represented on the actual serpentine path. The key architectural feature is the division between early vertical redistribution and DCV2-DCS region, which operates on the flow having previously passed through the offset path. The layout helps to explain why the further analysis treats the factors as position-specific geometric constraints, instead of substitutable levels codes. The first three codes presented in the lower half of the picture provide an early hint about the design: Configurations 3, 5, and 9 maintain A1 code, while their C-D codes still look good.

This visual hint is tested quantitatively in the results of factor-level analysis instead of being taken for granted based on the geometry.

2.2. Aerodynamic coefficients and retention scale

Three aerodynamic coefficients are the pressure recovery, discharge coefficient, and axial thrust coefficient. The pressure recovery, r_P, describes the fraction of stagnation-pressure quality recovered in the passage. The discharge coefficient, C_d, describes how well the nozzle produces mass flow in comparison with the reference flow. The axial thrust coefficient, C_f, describes how well the resulting flow produces axial momentum. In an offset nozzle, the three quantities are independent of each other. It is possible to have a sustained mass flow with the skewed exit velocity distribution. It is possible to have the sustained thrust direction without pressure recovery. Therefore, the three aerodynamic coefficients should be considered separately until the retention stage.

The raw response for configuration i and coefficient j is denoted by x_{ij}, where $j \in \{r_P, C_d, C_f\}$. The retention of the coefficient is defined by

$$R_{ij} = \frac{x_{ij} - x_j^{\min}}{x_j^{\max} - x_j^{\min}}, \qquad 0 \le R_{ij} \le 1. \tag{1}$$

The transformation in Eq. (1) maps the weakest observed value of the coefficient to 0 and the strongest observed value to 1 for every aerodynamic coefficient. The transformation does not reorder configurations for every coefficient. The purpose of the transformation is to bring the three coefficients to the common retention scale. This way, the unit change of R_{r_P}, R_{C_d}, or R_{C_f} has the same bounded interpretation.

The coefficient preservation index is the geometric mean of three retention values:

$$\mathrm{CPI}_i = \left(R_{i,r_P} R_{i,C_d} R_{i,C_f}\right)^{1/3}. \tag{2}$$

The geometric mean is used because it penalizes a weak component more strongly than an arithmetic average. This property is appropriate for coefficient preservation: if one retained coefficient is near zero, the configuration should not be described as a strong simultaneous-preservation candidate even if the other two retained coefficients are moderate. The lower-tail retention value is defined as

$$L_i = \min\left(R_{i,r_P}, R_{i,C_d}, R_{i,C_f}\right), \tag{3}$$

and the response-spread descriptor is defined as

$$S_i = \max\left(R_{i,r_P}, R_{i,C_d}, R_{i,C_f}\right) - \min\left(R_{i,r_P}, R_{i,C_d}, R_{i,C_f}\right). \tag{4}$$

The three numbers perform different functions. CPI assesses the overall retention rate, L ensures no weak retained coefficient, and S signals an imbalance in the retained coefficients' triad. High CPI with a low L indicates compensation. Low S with moderate CPI indicates balance without very high overall retention. The configuration of interest will excel in both aspects: have high overall value and not conceal a weak coefficient.

The calculation summary in Figure 2 shows the transition from the scales of raw coefficients to the common retention space. The three vertical scales make it evident that the numerical intervals are not identical: the interval of C_f and C_d is broader than the interval of r_P. The retention triangle is then an indication of the balance among the three retained coefficients. It is important since a nozzle having a strong coefficient and two weaker ones will be placed in a different area in the triangle compared to a nozzle with three high retained coefficients. Thus, the CPI, L, and S values are not duplicates since each of them introduces an additional check on the preservation hypothesis.

Preservation classes are established by a two-condition rule. Class I is the one requiring CPI $\geq$ 0.90 and $L \geq 0.85$. Class II includes configurations that possess CPI $\geq$ 0.75 and $L \geq 0.70$, but do not satisfy the requirements of Class I. Class III comprises the configurations having CPI $\geq$ 0.60 and $L \geq 0.55$ and do not belong to Class I or Class II. All other configurations are Class IV. Such values are applied as engineering filters, but not statistical confidence intervals. The reason for that is the design-oriented character of the analysis where a configuration should retain a high portion of each coefficient before being recognized as the best one.

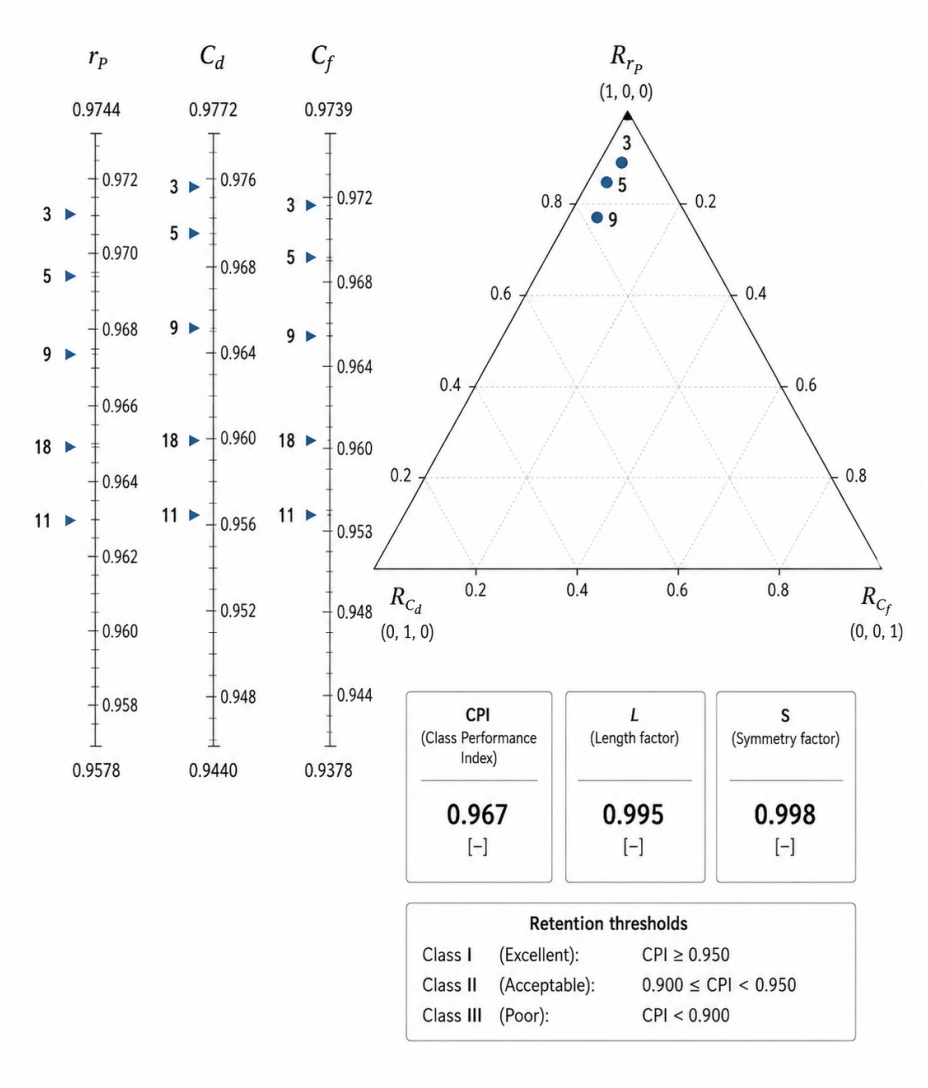

Figure 2. Retention calculation.

The class thresholds are designed as a pair of the parameters instead of being separate. In particular, a single CPI threshold would be rewarding a high geometric mean even when there is one weak coefficient. Similarly, the lower-tail threshold would be selecting configurations having good balance, but mediocre values of the retained coefficients. Hence, the two-condition rule asks two questions at once: is the candidate globally strong and is its weakest coefficient still acceptable? This combination is quite appropriate for the problem of the nozzle since all three characteristics are needed for the justified design of an exhaust system.

The spread descriptor S does not play the role of a strict class criterion, but it is kept for interpretational purposes since it clarifies the reasons for the difference in engineering importance between the configurations having a similar CPI value. Configurations having

CPI close to 0.90 and a very small spread are balanced and can be further refined. Configurations having the same CPI and high spread are more complicated since they have a weak spot, which will be essential if the operational conditions are changed.

2.2.1. Contrasts for factors and ranks' persistency

For each factor $F \in \{A, B, C, D\}$ and level $\ell \in \{1, 2, 3\}$ the factor-level preservation mean value is defined as

$$\overline{\mathrm{CPI}}_{F\ell} = \frac{1}{n_{F\ell}} \sum_{i \in F\ell} \mathrm{CPI}_i, \tag{5}$$

where $F\ell$ denotes the set of all indices in factor F on level ℓ. The level range $\Delta_F = \max_\ell \overline{\mathrm{CPI}}_{F\ell} - \min_\ell \overline{\mathrm{CPI}}_{F\ell}$ serves as a measure of factor contrast. Large contrast implies strong change of preservation property within the levels of a factor. Small contrast suggests a weakness, near-inactivity or interaction dependence of the factor. The computation of contrast is deliberately kept simple since its aim is interpretability – the reader can understand what distribution control moves the CPI envelope most without resorting to any complex selection model.

Ranks' persistency is evaluated by removing each coefficient in turn and recalculating the geometric preservation rank using only the other two coefficients. Thus, three additional ranks are generated: with the absence of r_P, with the absence of C_d and with the absence of C_f. The maximal shift from the rank of the full triad of coefficients is registered. This computation follows the spirit of sensitivity checking rather than some uncertainty quantification technique. The question addressed is whether the configuration is supported by its position in the response triad or is sensitive to the omission of one aerodynamic coefficient. High-rank configuration with zero rank mobility is better-defended compared to that of the same rank but strongly depending on the coefficient subset.

Thus, four interconnected outputs of this procedure include: the retention table, the preservation class of each configuration, the map of means of CPI over factor-levels and the ranks' persistency check. Each output provides answer to a particular aspect of the design question. The retention table gives information about the numerical state of every nozzle. The class rule selects the high-preserving subset. The factor means give explanation of how the coded distributions form the subset. The ranks' persistency check evaluates the robustness of the leading order against the change of the coefficient combination. All these steps make it possible to interpret the L27 matrix as the aerodynamic selection problem rather than the list of coefficient values.

The full appendix continues to play its role because it keeps the leading cases from isolation from the matrix body. Thus, the reader can ensure himself that the high-preserving candidates are not selected out by omission of inconvenient configurations or their compression from the lower part of the matrix. Moreover, the reader can see that the weakest case – Configuration 22 – defines the zero-retention point for all three coefficients while the Configuration 3 defines the unity point. Thus, the method becomes completely transparent from the raw coefficient table till the class assignment.

3. Results and discussion

3.1. Response scale and preservation classes

The original aerodynamic coefficients take on a restricted range of values, shown in Table 2. Pressure recovery ranges between 0.9578 and 0.9744, discharge coefficient between 0.9440 and 0.9772, and axial thrust coefficient between 0.9378 and 0.9739.

Table 2. Response scale.

Criterion	Minimum	Maximum	Span	Mean	SD
r_P	0.9578	0.9744	0.0166	0.9666	0.0043
C_d	0.9440	0.9772	0.0332	0.9630	0.0094
C_f	0.9378	0.9739	0.0361	0.9578	0.0099

This shows why a preservation-class-based scale can be beneficial in the present context. The numerical span of C_f is greater than that of r_P, and that of C_d is greater than that of pressure recovery. If the coefficients were to be directly summed up in the aggregation step, a larger numerical span would dominate the results due to its numerical strength, despite the equal aerodynamic importance of all three responses. Standardization of each response prior to the aggregation step allows avoiding this problem and distinguishing between uniform and partial coefficient retention.

The data also show that small changes are significant and should not be dismissed. A difference in pressure recovery of 0.010 may seem small compared to unity, but it is a great portion of the observed range of r_P values in the L27 nozzle matrix. The same holds true for the discharge and thrust coefficients. The retention transformation thus considers each response with respect to the range of variation in the given matrix. It is proper to a design problem since the aim here is not to compare the nozzle to an ideal nozzle but to select the best nozzle from the investigated set.

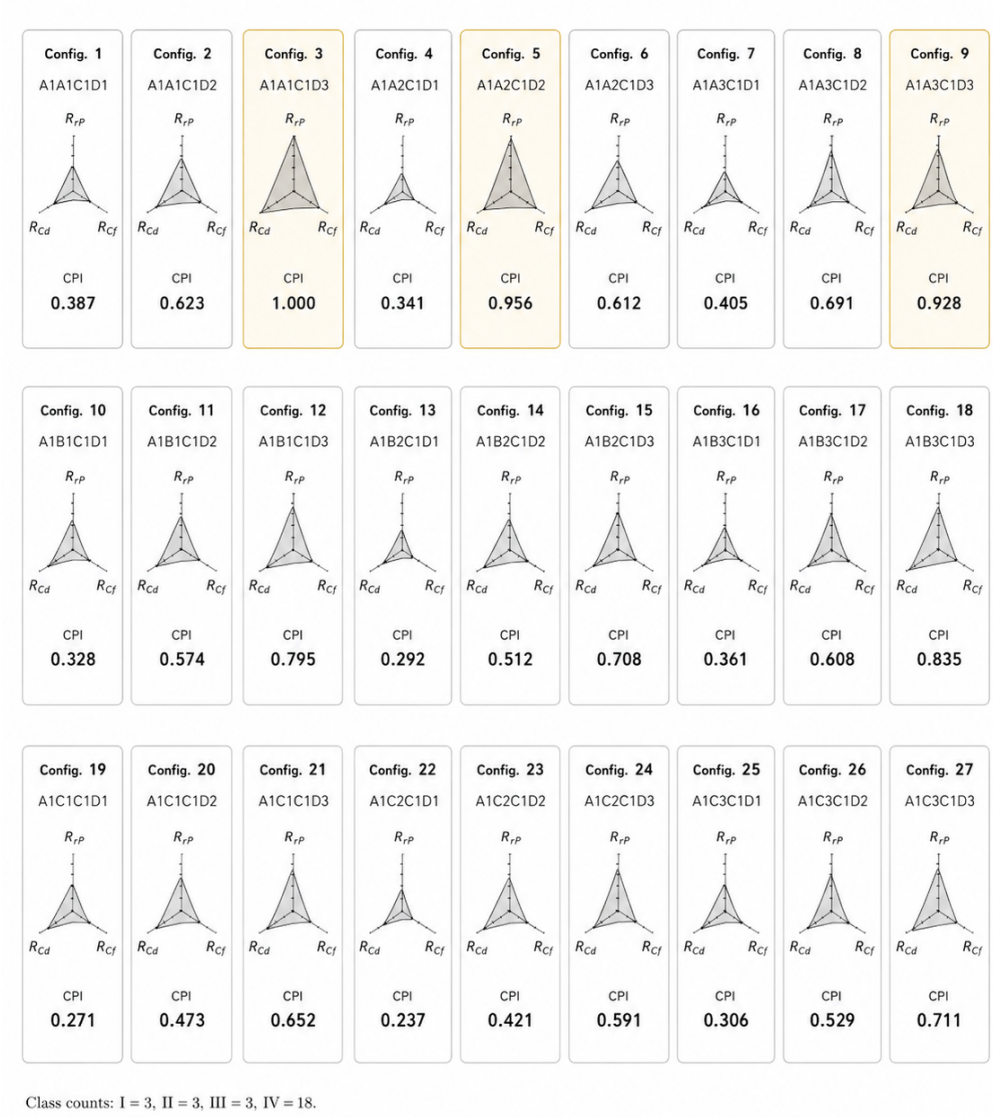

Figure 3. Configuration fingerprints.

The configuration fingerprint wall in Figure 3 shows the shapes of coefficient retention in all 27 configurations with the same triad geometry so that the reader could examine the

shape of the triad rather than just ranks of preservation of individual responses. Configurations 3, 5, and 9 have a broadly-filled triad while the lower-ranked candidates display either contracting or asymmetrical shapes. The difference between configurations is valuable since it reveals whether the CPI value of a candidate relies upon the simultaneous preservation of all three coefficients or a different response profile. A broad triangular fingerprint corresponds to the good values of pressure recovery, discharge coefficient, and thrust coefficient in comparison to their respective maxima. On the other hand, a contracted or asymmetrical fingerprint implies that at least one coefficient has become a bottleneck of the CPI score.

The all-configurations layout also illustrates the selectivity of the high-PRI region since the top-ranked candidates are clustered within a small part of the matrix rather than randomly distributed throughout all 27 configurations. The configurations with poor CPI values often demonstrate both a narrow shape and a contraction asymmetry of the footprint, implying that the poor overall retention is linked with a visible imbalance in the triad of coefficients. This gives another reason to prefer CPI+lower tail approach over CPI analysis only since a candidate needs not only a high CPI but also a balanced retention triad.

The preservation classes in Table 3 reveal the distribution of configurations among the four groups defined with thresholds. There are only three configurations in Class I and eighteen out of twenty-seven configurations belong to Class IV.

Table 3. Preservation classes.

Class	Count	Share (%)
Class I	3	11.1
Class II	3	11.1
Class III	3	11.1
Class IV	18	66.7

The class counts serve as valuable information since it proves that the area of high-preservation is selective. A wide selection plateau would lead to the creation of many Class I or Class II candidates. However, the class counts prove that there are no such candidates and the dominant class is Class IV; thus, design guidance can be obtained based on the common factors of only a small number of successful cases instead of averaging the whole matrix. The equal counts in Classes I, II, and III should not be viewed as a linear progression in terms of performance. Instead, they represent the threshold values determined by two criteria – CPI and lower-tail retention. It means that in engineering terms many configurations fail because of the weakness of one of the coefficients and not because the aggregate value is slightly below a particular target.

At the same time, the presence of low-preservation cases is another proof that the average-only approach cannot work. Since there are eighteen configurations classified as Class IV, the average value will be influenced by the geometry, which is unsuitable for the coefficient-preserving operations. For this reason, it is necessary to use only the configurations in upper classes as the base for comparison. Configurations 3, 5, 9, 18, and 11 determine the practical border between the cases that allow coefficient preservation and lower-tail limitation. Other configurations also contribute to the factor-level interpretation but should not distract from the main point.

The class structure is also a sign that the matrix includes a clear selection gradient rather than random numerical data. Only the configurations with high aggregate CPI and lower-tail retention belong to Class I. There are other useful but less efficient configurations in Class II. Class III includes partially preserved configurations without adequate high-end preservation. Class IV consists of the configurations with a poor retention signature. Such hierarchy is valuable since it transforms a mere numerical table into the engineering decision.

3.2. Leading configurations

Configurations with the top twelve ranks are presented in Table 4. Complete retention in all three coefficients is achieved by Configuration 3. Configurations 5 and 9 are still in Class I, while Configurations 18, 11, and 2 are Class II candidates, as their lower-tail retention is above 0.70, however, CPI values are below the Class I threshold.

Table 4. Leading candidates.

Config.	Combination	R_{r_p}	R_{C_d}	R_{C_f}	CPI	L	S	Class
3	A1B1C3D3	1.000	1.000	1.000	1.000	1.000	0.000	Class I
5	A1B2C2D3	0.934	0.985	0.950	0.956	0.934	0.051	Class I
9	A1B3C3D2	0.892	0.970	0.925	0.928	0.892	0.078	Class I
18	A2B3C3D3	0.843	0.946	0.909	0.898	0.843	0.102	Class II
11	A2B1C2D3	0.777	0.870	0.859	0.834	0.777	0.093	Class II
15	A2B2C3D2	0.741	0.855	0.837	0.809	0.741	0.114	Class III
2	A1B1C2D2	0.771	0.825	0.812	0.802	0.771	0.054	Class II
24	A3B2C3D3	0.590	0.780	0.753	0.703	0.590	0.190	Class III
17	A2B3C2D2	0.602	0.780	0.717	0.696	0.602	0.178	Class III
26	A3B3C2D3	0.518	0.762	0.701	0.652	0.518	0.244	Class IV
6	A1B2C3D1	0.741	0.593	0.601	0.642	0.593	0.148	Class IV
21	A3B1C3D2	0.458	0.675	0.665	0.590	0.458	0.217	Class IV

The table of leading candidates provides a sharper answer than a simple first-place statement. Configuration 3 is the only full retention case. Configuration 5 possesses the maximum residual balance out of the followers, CPI = 0.956 and lower-tail retention = 0.934. Configuration 9 remains a good Class I configuration, but it possesses lower pressure-recovery retention than Configuration 5. Configuration 18 is close to the high preservation boundary, however, due to lower-tail pressure-recovery retention value of 0.843, it is classified as non-Class I according to the stated rule. This changes the engineering interpretation of the results: Configuration 18 is the strong alternative configuration, however, it is not equivalent to the three high-retention cases.

The combination codes of the leading cases provide the additional physical information. Three Class I cases all contain A1, thus highlighting the importance of the chosen area-distribution schedule. Configurations 3 and 9 have C3, and Configurations 3 and 5 possess D3, hence demonstrating the importance of the strongest region in connection with downstream distribution choice rather than with any universal factor level combination. DCV1 of the three leading configurations differs: B1 in Configuration 3, B2 in Configuration 5, and B3 in Configuration 9. It is the initial hint on the fact that DCV1 is not the separating variable of the high-preservation region, a conclusion supported by factor-level means of the further analysis.

Figure 4 presents the preservation gate showing the reason why the class definition cannot be reduced to CPI alone. Configurations 3, 5, and 9 reside in the upper-right region of acceptance, while Configuration 18 lies just below the lower-tail limit despite its relatively high total CPI value. Hence, the selection criterion becomes clear: the configuration should preserve the weakest coefficient along with possessing high CPI. Location of Configuration 18 is especially informative in this regard because it is located close to the accepted region. Thus, the reason for its exclusion is not low total CPI but low lower-tail retention allowing weak coefficient to hide behind two stronger retained coefficients.

Combined reading of Table 4, Figure 3 and Figure 4 demonstrates that the leading set of configurations is not the single-point result. Configuration 3 is the complete reference case, Configuration 5 is the most balanced follower, and Configuration 9 is accepted because the weakest of its retained coefficients remains above the high-preservation limit. Configurations 18 and 11 should be considered as stable alternatives rather than members of the preferred high-preservation set. The latter is important from the viewpoint of future

engineering work: Class II alternative configuration can be used for comparison, but should not be treated as equivalent to the Class I candidate under the necessity to retain three coefficients.

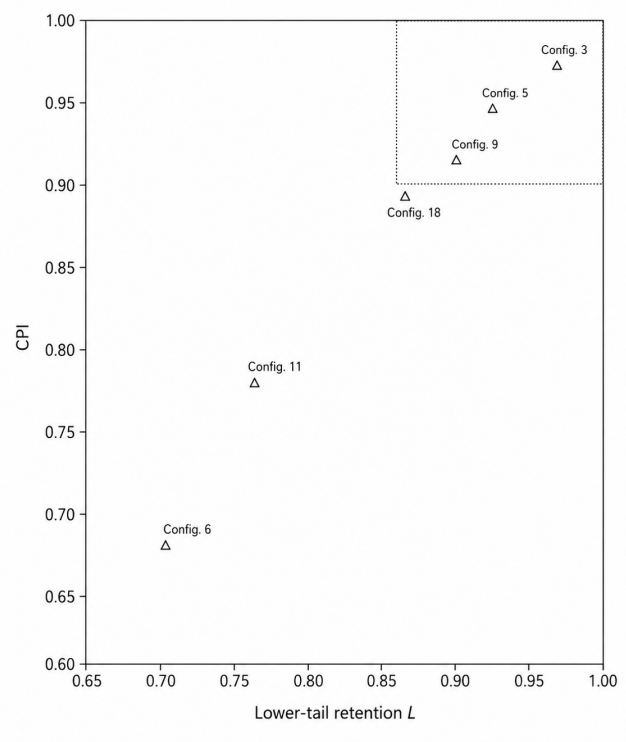

Figure 4. Preservation gate.

The comparison of Configurations 5 and 9 is informative because these configurations are both accepted but not interchangeable. Configuration 5 possesses slightly higher CPI value and smaller spread, hence retaining more evenly balanced coefficient triad. Configuration 9 has stronger downstream vertical setting but weaker pressure-recovery retention value. Thus, if the next design phase stresses the uniformity across pressure recovery, discharge and thrust, Configuration 5 will be the more conservative follower to Configuration 3. However, if the next design phase investigates the influence of C3 setting on downstream redistribution, Configuration 9 will remain the important Class I case.

Configuration 18 provides the most informative near miss. Its CPI value of 0.898 is close to the limit of Class I, and the configuration has a stable rank, however, its lower-tail value of 0.843 falls below the required limit of 0.85. The difference is small in numerical terms but is very significant from the methodological point of view. Without the lower-tail criterion, Configuration 18 would be difficult to distinguish from the preferred configuration set. With this criterion, the article clearly states the reasons for considering the configuration as the secondary option: the weakest of the retained coefficients does not quite reach the high-preservation level. Exactly such a distinction is necessary during compact nozzles selection under multiple aerodynamic criteria.

3.3. Factor-level interpretation

Factor-level CPI means are provided in Table 5. The second vertical distribution (C) shows the largest preservation range, followed closely by the spanwise distribution (D). The area distribution (A) displays a moderate range, while the first vertical distribution (B) is almost constant.

From the factor means, it can be seen that the dominant geometric mechanism in the present matrix is DCV2, which grows from CPI 0.295 (L1) to CPI 0.716 (L3) and DCS, which rises from CPI 0.353 (L1) to CPI 0.706 (L3). Both factors display large variations on the

response scale. On the other hand, the variation of DCV1 is 0.011, which indicates that its effect is relatively weak on average for all the other factor levels. The resulting preservation rule is, thus, a preference for the Level 3 position in the downstream vertical and spanwise distributions with the Level 1 area distribution.

Table 5. Factor CPI means.

Code	Factor	Level 1	Level 2	Level 3	Range	Best level
A	DA, area distribution	0.680	0.574	0.393	0.287	L1
B	DCV1, first vertical distribution	0.542	0.553	0.552	0.011	L2
C	DCV2, second vertical distribution	0.295	0.636	0.716	0.420	L3
D	DCS, spanwise distribution	0.353	0.588	0.706	0.353	L3

Also relevant is the opposite performance of A relative to C and D. DA performs best at Level 1, while DCV2 and DCS perform best at Level 3. In other words, good preservation is not achieved by selecting the same level for every factor; in fact, the area schedule and downstream centerline schedules seem to fulfill complementary aerodynamic tasks. While A1 may help keep the acceleration-pressure recovery pattern favorable in the early part of the passage, C3 and D3 may help shape the already redistributed flow as it approaches the extension.

In the leverage diagram of Figure 5, the contrast structure becomes evident without obscuring the level sequence. The track of factor B is flat, while the tracks of C and D rise steeply to the third level. This result is consistent with the physical process of sequential turning, where the downstream vertical and spanwise redistributions act after the curvature effects have introduced flow nonuniformity, and so their level placement is crucial in determining the preservation performance. The influence of area distribution remains but its best level is different from those of C and D; it implies that acceleration scheduling and downstream centerline placement complement each other.

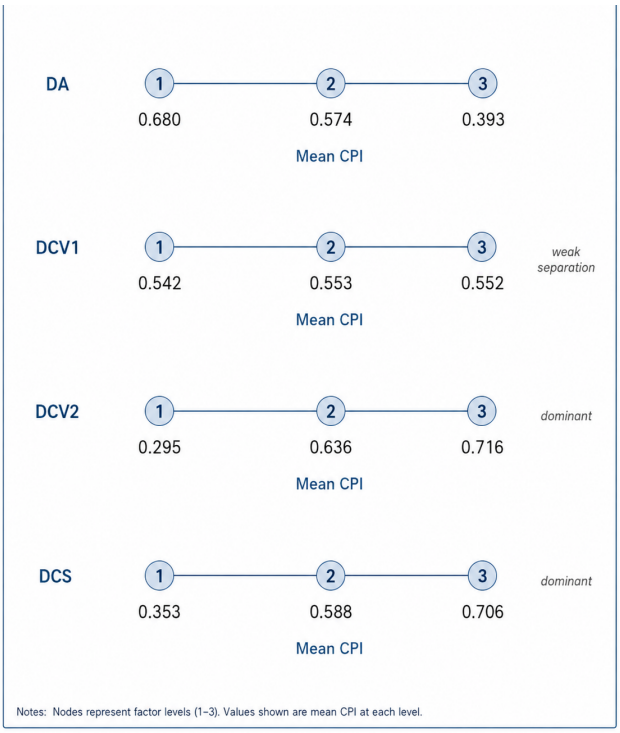

Figure 5. Factor leverage.

However, it should be taken into account that the flatness of the B track does not imply that the first vertical redistribution does not have any aerodynamic significance in every

possible nozzle. The weak trend means only that, within the current L27 family and with the three selected coefficients, there is no significant average effect of changing DCV1 from Level 1 to Level 2 or Level 3. The most successful configurations support this interpretation because B1, B2, and B3 are included in the three Class I cases; in contrast, the strongest cases do not give the same freedom in A, C, and D. This factor-level result separates a design variable with flexible behavior from more decisive ones.

The magnitude of the ranges of C and D provides practical priority to downstream geometric control. DCV2 shows the largest range, 0.420, followed by the second largest range of DCS with 0.353. Neither value can be considered as a minor perturbation; they occupy a substantial part of the CPI scale. So, a designer working with the current table would achieve more from adjusting a bad choice of C or D than from fine-tuning DCV1. This result is consistent with the expected aerodynamic importance of downstream geometry in controlling the final delivery of the passage flow.

3.4. Rank mobility under response elimination

Results of leave-one-response tests are shown in Table 6. Five top configurations in terms of priority preserve their ranks after exclusion of any one of r_P, C_d, and C_f.

Table 6. Rank mobility.

Config.	Full rank	Without r_P	Without C_d	Without C_f	Max shift
3	1	1	1	1	0
5	2	2	2	2	0
9	3	3	3	3	0
18	4	4	4	4	0
11	5	5	5	5	0
15	6	6	7	7	1
2	7	7	6	6	1
24	8	8	9	9	1
17	9	9	10	8	1
26	10	10	11	11	1
6	11	12	8	10	3
21	12	11	14	14	2

Mobility analysis confirms the preservation-based conclusion about the reliability of the top-five set of designs. Only after the sixth configuration the change of local order occurs depending on which one of the coefficients is eliminated. This result is not surprising since in the middle part of the list the coefficients' values of the candidates are close enough for the change of ordering upon a minor change of definition of the objective. In the case of the first five positions this condition is satisfied due to sufficient separation between those configurations and balance in their coefficients.

Zero value of mobility does not imply that the five leading configurations are equally good candidates. Configurations 3, 5, and 9 reach the Class I threshold, whereas Configurations 18 and 11 do not. The mobility test provides an answer to a different question, namely whether the rank depends on inclusion of one of the coefficients in it. A configuration can be stable in terms of its rank without reaching the Class I criterion. That is why the article uses multiple criteria to validate the top five candidates. The criteria of CPI, L, factor contrast and rank mobility prevent a different misinterpretation of the same table of coefficients.

Figure 6 illustrates the rank ribbons as a simple stability check of the configuration ranks. The straight line for Configurations 3, 5, 9, 18, and 11 indicates full stability of their rankings under response removal. Obvious exchange of the configurations 6 and 21 shows that the candidate can be found relatively high in the list, yet it is more sensitive to which aerodynamic response is considered important. This difference is useful for design selection, since stable second-class candidate can be more preferable than its competitor

which position is changed drastically due to a minor redefinition of the performance objective.

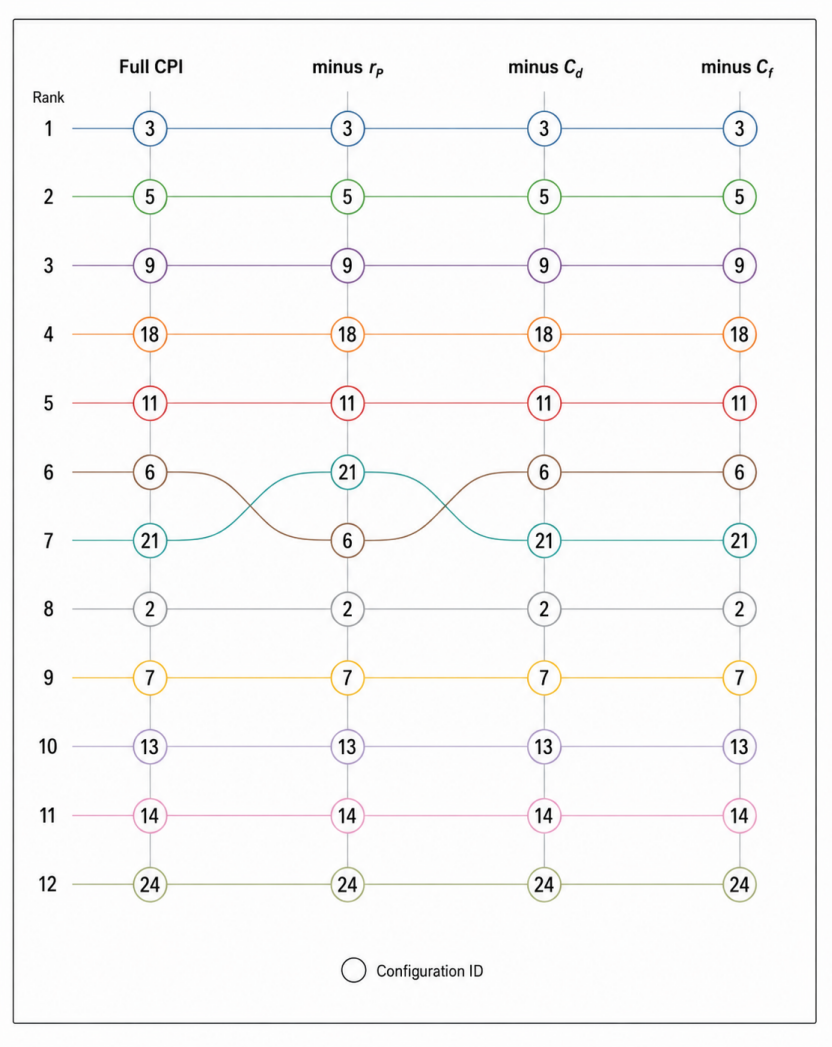

Figure 6. Stable ranking core.

Finally, mobility analysis gives confidence that the leading order is not defined by the span of the coefficients' numerical values only. If the discharge coefficient or axial thrust coefficient were dominating the triad simply because they have wider raw spans, then the elimination of either quantity should have led to the disturbance of the leading ranks. Zero value of mobility for the first five candidates proves that their ordering is determined by all three of the coefficients in the triad. Thus, the above statement about the genuine simultaneous-preservation of the Class I set of configurations holds true.

3.5. Implications for aerodynamics

The analysis has a straightforward physical meaning. The best configurations consist of an exit-focused area distribution (A1) and entrance-focused downstream vertical or spanwise redistribution (C3 and/or D3). Such a combination allows maintaining the coefficient triad in balance through acceleration scheduling and downstream turning positioning. In a double-serpentine passage, the downstream domain is where the influence of prior curvatures has been already built into velocity and pressure distributions. Hence, an advantageous downstream redistribution may weaken skewness propagation to the extension and exit plane, while an unfavorable one may exacerbate a preexisting nonuniformity.

The lack of significance of DCV1 does not imply that the first vertical turn is always physically insignificant. It is conditional on the fixed L27 envelope. In this envelope, variations of DCV1 do not differentiate the configurations nearly as much as variations of DCV2 and DCS. The reason behind this lies in the fact that early turning comes before the full history of the serpentine is formed, and later redistributions have direct control over the state delivered to the exit section. As seen from the leading set, B can vary without preventing high preservation levels, while A1 and favorable C/D selections are key.

The coefficient-preservation consideration is useful for determining the hierarchy of design preferences. The Class I cases are good for confirming the flow field because they preserve all three global aerodynamic coefficients. The Class II cases provide useful alternates but should be inspected for their weakest coefficient before being chosen. The Class III and IV cases may also provide useful information about factor influences, but they cannot be considered good choices for preservation-based design. This hierarchy circumvents the frequent pitfall of single-score optimization, where an option can be promoted despite the unknown acceptability of its weakest aerodynamic performance.

The selection map in Figure 7 summarizes the design implication of the analysis. Configurations 3, 5, and 9 lie in the favorable center since they satisfy the coefficient-adequacy, balance, and rank-persistence conditions together. Configurations 18 and 11 continue being useful alternatives but with weaker lower-tail behavior and thus should not be used as equal to the set of high-preserving configurations. In this way, the map represents the geometry preference resulting from the numerical analysis: A1 together with downstream-oriented C/D selection.

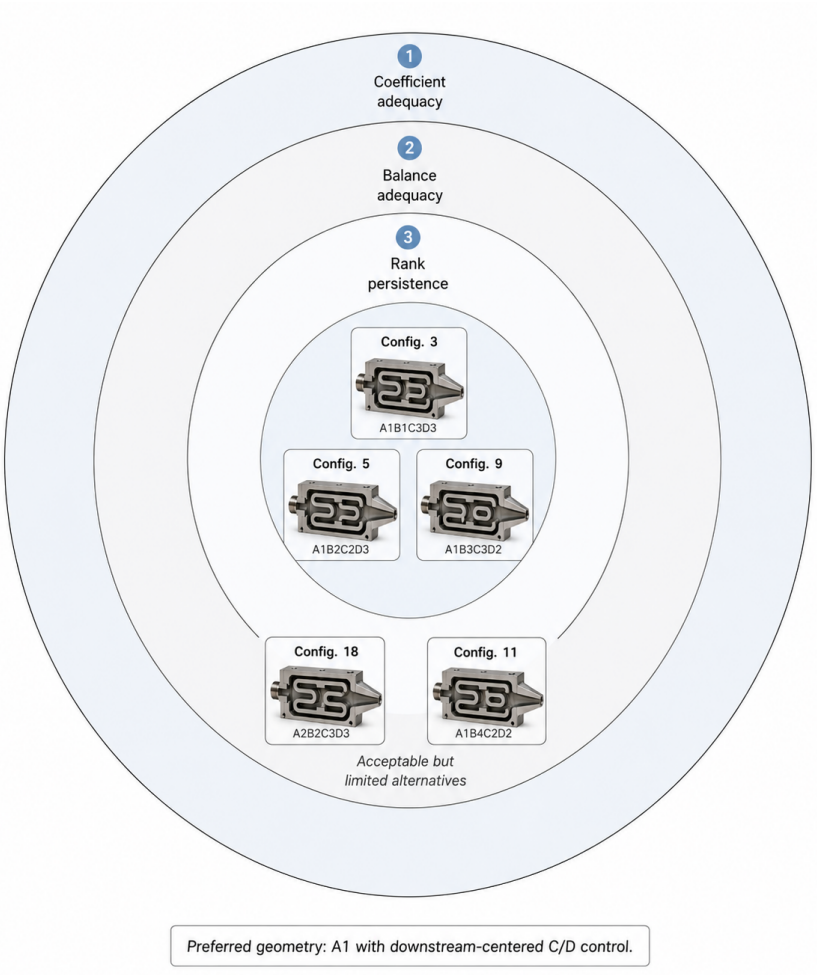

Figure 7. Selection map.

The design rule can be stated operationally. If the target is the most reliable coefficient-preserving nozzle from the family investigated, then Configuration 3 should be selected first since it preserves all three coefficients at their maxima. If there is a need in some alternative, Configuration 5 is the strongest follower with small retention spread and high lower tail value. Configuration 9 can be considered the third choice but with a more evident loss of pressure recovery. Configurations 18 and 11 are good for comparison but should not substitute the Class I set when the weakest coefficient is a limit requirement.

In addition, this result indicates the direction for future aerodynamic analysis. Since the most influential factor contrast lies in DCV2 and DCS, the detailed flow study should be performed for understanding how the second vertical and spanwise redistributions affect pressure gradients, strength of secondary flows, wall separation, and exit plane velocity orientation. The global coefficients alone define the successful cases, but the physical mechanism behind the success will become clearer from the local flow quantities. Thus, the current coefficient-preservation analysis provides the basis for further flow-field analysis without weakening the current result.

4. Conclusions

The key governing question was which offset double-serpentine nozzle configurations preserve pressure recovery, discharge coefficient, and axial thrust coefficient simultaneously, and what factor combinations delineate the high-preservation region in the design space. The answer is precise and numerical. Configurations 3, 5, and 9 are the only cases preserving CPI $\geq$ 0.90 and lower-tail retention $\geq$ 0.85 at the same time. Configuration 3 is the sole full-preservation nozzle, with all normalized coefficients being unity. Configuration 5 is the best follower case because it is a combination of CPI = 0.956 and lower-tail retention = 0.934 with retention spread of 0.051. Configuration 9 also preserves CPI = 0.928, even though its pressure-recovery retention is worse compared to Configuration 5.

The factor-level answer is equally precise. DCV2 and DCS delineate the leading preservation envelope, with mean CPI range of 0.420 and 0.353 correspondingly. DA has moderate influence, with a mean CPI range of 0.287, and DCV1 is almost inactive in average CPI along the matrix, with range of just 0.011. High preservation correlates with A1, C3, and D3-level choices, implying that the area schedule and downstream centerline distributions should be considered in a coordinated way rather than separately. The answer is not a general rule that all factors have to tend to the same level; it is the level-specific answer for the investigated double-serpentine geometry.

The rank-persistence test shows that the leading five configurations do not depend on any single aerodynamic coefficient. Their ranks are constant under exclusion of pressure recovery, discharge coefficient, or axial thrust coefficient from the ranking computation. This stability justifies the use of preservation classes as a quantitative criteria of nozzle configuration selection. On the other hand, the distinction between Class I and Class II is also valid: Configurations 18 and 11 are stable alternatives, but do not have the same lower-tail strength as Configurations 3, 5, and 9. Rank stability strengthens the interpretation without supplanting the lower-tail requirement.

Therefore, the practical answer is obvious. Configuration 3 is to be considered as the key coefficient-preserving nozzle in the investigated family. Configuration 5 is to be retained as the best balanced alternative, and Configuration 9 is to be retained as the third high-preservation member. Configuration 18 is to be used as the boundary case for the study of effects of slightly deficient lower-tail value. Four case set provides a narrow path for any subsequent resolved-flow study: one case of complete preservation, two cases of accepted alternatives, and one near-boundary case for comparison.

The main design implication is that the compact offset double-serpentine nozzle has to be considered based on the weakest retained coefficient in addition to overall performance. A single favorable coefficient or a single composite value is not sufficient in cases when pressure recovery, discharge coefficient, and axial thrust have to be preserved at once. In the framework of the present L27 family, the optimal design route is an A1 area schedule

along with DCV2 and DCS favorable distributions. This route ensures the protection of the coefficient triad through the coordination of early area scheduling and downstream redistribution control. Further detailed investigation of the flow field is to correlate the coefficient classes with separation degree, secondary flows, exit-plane swirl, and thermal signature, but the current numerical answer is already definitive in relation to the posed coefficient-preservation problem.

The conclusion is deliberately restricted to the listed coefficient table and coded nozzle geometry. The values are not universal optima for all serpentine nozzles, but give a comprehensive answer for the investigated family. The numerical boundary is particularly useful since it identifies not only the preferred cases, but also the first cases to be rejected in cases of simultaneous coefficient preservation requirements.

The final recommendation is not the nozzle shape preference, but the coefficient-confirmed selection quantitatively justified by the L27 arrangement, the class boundary, the factor contrast, and the response removal test.

Data availability

Table 7 contains the complete numerical table used for all calculations in the article.

Table 7. Complete numerical table.

Config.	Combination	r_P	C_d	C_f	CPI	L	Class	Rank
3	A1B1C3D3	0.9744	0.9772	0.9739	1.0000	1.0000	Class I	1
5	A1B2C2D3	0.9733	0.9767	0.9721	0.9560	0.9337	Class I	2
9	A1B3C3D2	0.9726	0.9762	0.9712	0.9283	0.8916	Class I	3
18	A2B3C3D3	0.9718	0.9754	0.9706	0.8982	0.8434	Class II	4
11	A2B1C2D3	0.9707	0.9729	0.9688	0.8344	0.7771	Class II	5
15	A2B2C3D2	0.9701	0.9724	0.9680	0.8094	0.7410	Class III	6
2	A1B1C2D2	0.9706	0.9714	0.9671	0.8023	0.7711	Class II	7
24	A3B2C3D3	0.9676	0.9699	0.9650	0.7027	0.5904	Class III	8
17	A2B3C2D2	0.9678	0.9699	0.9637	0.6960	0.6024	Class III	9
26	A3B3C2D3	0.9664	0.9693	0.9631	0.6516	0.5181	Class IV	10
6	A1B2C3D1	0.9701	0.9637	0.9595	0.6417	0.5934	Class IV	11
21	A3B1C3D2	0.9654	0.9664	0.9618	0.5900	0.4578	Class IV	12
7	A1B3C1D3	0.9677	0.9625	0.9566	0.5573	0.5208	Class IV	13
8	A1B3C2D1	0.9682	0.9616	0.9563	0.5542	0.5125	Class IV	14
12	A2B1C3D1	0.9672	0.9601	0.9559	0.5164	0.4849	Class IV	15
23	A3B2C2D2	0.9639	0.9643	0.9581	0.5018	0.3675	Class IV	16
13	A2B2C1D3	0.9658	0.9592	0.9543	0.4655	0.4571	Class IV	17
14	A2B2C2D1	0.9661	0.9583	0.9533	0.4522	0.4294	Class IV	18
4	A1B2C1D2	0.9659	0.9585	0.9528	0.4457	0.4155	Class IV	19
27	A3B3C3D1	0.9627	0.9575	0.9511	0.3536	0.2952	Class IV	20
10	A2B1C1D2	0.9636	0.9552	0.9500	0.3415	0.3373	Class IV	21
19	A3B1C1D3	0.9618	0.9542	0.9493	0.2868	0.2410	Class IV	22
20	A3B1C2D1	0.9619	0.9536	0.9481	0.2731	0.2470	Class IV	23
1	A1B1C1D1	0.9637	0.9497	0.9452	0.2321	0.1717	Class IV	24
25	A3B3C1D2	0.9596	0.9522	0.9450	0.1748	0.1084	Class IV	25
16	A2B3C1D1	0.9611	0.9487	0.9424	0.1531	0.1274	Class IV	26
22	A3B2C1D1	0.9578	0.9440	0.9378	0.0000	0.0000	Class IV	27

References

[1] Dean, W. R. Note on the motion of fluid in a curved pipe. *The London, Edinburgh, and Dublin Philosophical Magazine and Journal of Science* **1927**, *4*(20), 208–223.

[2] Pope, S. B. (2001). Turbulent flows. Measurement Science and Technology, 12(11), 2020-2021.

[3] Bansod, P., & Bradshaw, P. (1972). The flow in S-shaped ducts. Aeronautical Quarterly, 23(2), 131-140.

[4] Guo, R. W., & Seddon, J. (1982). An investigation of the swirl in an S-duct. Aeronautical Quarterly, 33(1), 25-58.
[5] Bou-Zeid, E., Anderson, W., Katul, G. G., & Mahrt, L. (2020). The Persistent Challenge of Surface Heterogeneity in Boundary-Layer Meteorology: A Review: E. Bou-Zeid et al. Boundary-Layer Meteorology, 177(2), 227-245.
[6] Brunton, L. L., Hilal-Dandan, R., & Knollmann, B. C. (2017). McGraw-Hill Education: New York. NY, USA.
[7] Mattingly, J. D., Boyer, K. M., & von Ohain, H. (2006). Elements of propulsion: gas turbines and rockets (Vol. 53). Reston, VA: American Institute of Aeronautics and Astronautics.
[8] Wellborn, S. R., Reichert, B. A., & Okiishi, T. H. (1994). Study of the compressible flow in a diffusing S-duct. Journal of Propulsion and Power, 10(5), 668-675.
[9] Box, G. E., Hunter, J. S., & Hunter, W. G. (2005). Statistics for experimenters: design, innovation, and discovery. John Wiley & Sons.
[10] Myers, R. H., Montgomery, D. C., & Anderson-Cook, C. M. (2016). Response surface methodology: process and product optimization using designed experiments. John Wiley & Sons.
[11] Belton, V., & Stewart, T. (2012). Multiple criteria decision analysis: an integrated approach. Springer Science & Business Media.
[12] Köksalan, M. M., Wallenius, J., & Zionts, S. (2011). Multiple criteria decision making: from early history to the 21st century. World Scientific.
[13] Saltelli, A., Ratto, M., Andres, T., Campolongo, F., Cariboni, J., Gatelli, D., ... & Tarantola, S. (2008). Global sensitivity analysis: the primer. John Wiley & Sons.
[14] Sobol, I. M. (2001). Global sensitivity indices for nonlinear mathematical models and their Monte Carlo estimates. Mathematics and computers in simulation, 55(1-3), 271-280.
[15] Oberkampf, W. L., & Trucano, T. G. (2002). Verification and validation in computational fluid dynamics. Progress in aerospace sciences, 38(3), 209-272.